PERGAMON

International Journal of Heat and Mass Transfer 43 (2000) 2827–2839

International Journal of HEAT and MASS TRANSFER

www.elsevier.com/locate/ijhmt

Boundary information based diagnostics on the thermal states of biological bodies

Jing Liu, Lisa X. Xu*

Department of Biomedical Engineering, School of Mechanical Engineering, 1288 Mechanical Engineering Building, Purdue University, West Lafayette, IN 47907-1288, USA

Received 23 June 1999; received in revised form 5 November 1999

Abstract

Quantitative diagnostics on the thermal states of biological bodies and optimal dosimetry in tumor hyperthermia require general solutions for the bioheat equation. An algorithm based on the dual reciprocity boundary element method (DRBEM) is developed to solve the integral inverse or direct bioheat transfer problems. Using this algorithm, thermal states of the biological bodies, reflecting physiological conditions, can be correlated to the temperature or heat flux detected at the skin surface. The extension of the algorithm to the non-linear bioheat model and boundary conditions is also discussed. Various cases are studied to illustrate its applications. This algorithm can be used as an effective tool for thermal diagnostics in medical practices.

Keywords: Bioheat transfer; Dual reciprocity boundary element method; Noninvasive diagnostics

1. Introduction

It has long been revealed that the body surface temperature is controlled by the blood circulation underneath the skin, local metabolism, and heat exchange between the skin and its environment [1–6]. Changes in any of these parameters can induce variations of temperature and heat flux at the skin surface, reflecting the physiological state of the human body. For example, a highly vascurized skin tumor can lead to an increase of local blood flow and thus to an increase in skin temperature. Temperatures at the skin above a breast tumor have been found to be several degrees higher than that of the surrounding area [5,6]. Inflammation-induced high metabolic rate can also increase the skin temperature. On the other hand, thrombosis or vascular sclerosis in the peripheral circulation decreases the blood flowing to the skin resulting in low skin temperatures. In burn injuries, low skin temperatures can occur due to insufficient blood supply. Apparently, the abnormal temperature or heat flux at the skin surface might indicate irregular peripheral circulation which can be used in clinical diagnosis.

Compared to other non-invasive thermometry like MRI, microwave, and ultrasound [6], thermal methods appear to be more economic and safer. The non-invasive diagnosis using skin surface temperature measurement is appealing if accurate correlations can be established. It requires solutions to inverse bioheat transfer problems which, however, has received much less attention [1,7–11], compared to studies on the

* Corresponding author. Tel.: 765-494-6637; fax: 765-494-0539.

E-mail address: lxu@ecn.purdue.edu (L.X. Xu).

0017-9310/00/$ - see front matter
PII: S0017-9310(99)00367-1

Nomenclature

c_p specific heat of tissue (J/kg °C)
c_b specific heat of blood (J/kg °C)
h_{eff} effective heat transfer coefficient (W/m^2 °C)
h_f convection heat transfer coefficient (W/m^2 °C)
h_r radiation heat transfer coefficient (W/m^2 °C)
k thermal conductivity of tissue (W/m °C)
q temperature gradient (°C/m)
q'' heat flux (W/m^2)
$\tilde{q}''_w$ constant surface heat flux oscillation amplitude (W/m^2)
Q_m metabolic rate of tissue (W/m^3)
Q_r spatial heating (W/m^3)
t time (s)
T tissue temperature (°C)
T_a artery temperature (°C)
T_{env} environmental background temperature (°C)
T_f fluid temperature (°C)
T_s skin surface temperature (°C)
x, y coordinate (m)

Greek symbols
ω heating frequency
ω_b blood perfusion rate (ml/s/ml)
φ phase shift (°)
ε emissivity of skin
σ Stefan–Boltzmann constant
α thermal diffusivity of tissue (m^2/s)
β internal angle at boundary point
Ω calculation domain
ρ density of tissue (kg/m^3)
ρ_b density of blood (kg/m^3)
θ temperature elevation of living tissues (°C)
θ_f relative temperature of flow
θ_q position parameter
θ_u position parameter
θ^* fundamental solution to Laplace equation

Secondary parameters
b $1/\alpha$
c $\omega_b \rho_b c_b / k$
d $-Q_r/k$

direct problems [12–21]. Among different minimal invasive approaches, the finite element method (FEM) has been well studied due to its good adaptability to complex shapes. Nevertheless, estimations of the thermal states have to be performed through numerous invasive temperature measurements inside tissue via inserted probes to determine blood perfusion [7]. Once the predicted temperatures based on an initially assigned perfusion are close enough to the measured at the probe locations, then the perfusion is regarded as the real value to be used. Other approaches like finite difference method (FDM) cannot osculate the coordinates of the complex biological shape. The direct approach used in [22] to estimate the 1D blood perfusion possessed relatively large errors resulting from the solution of the non-linear bioheat equation. Compared with the above approaches, BEM is regarded as an advantageous method due to its unique ability to provide a complete problem solution in terms of boundary values only, with substantial savings in computer time and data preparation [23,24]. Ren et al. [24] have applied BEM to identify the spatially distributed heat sources based on simultaneous measurements of temperature and heat flux at the skin surface. But their approach was for the steady state only. There exist severe restrictions in the traditional BEM for solving the bioheat transfer equation (BHTE). One is that the fundamental solution to the BHTE with non-homogeneous blood perfusion term is hard to obtain presently [23,24]. Thus the equivalent boundary integral equation is not available. And in most cases, it is inconvenient to alter the program by incorporating a new fundamental solution when the user wishes to study a slightly different bioheat equation. Further more, the non-homogeneous term accounting for spatial heating needs to be included in the ordinary BEM formulation by means of domain integrals, which makes the technique time consuming and lose the attraction of its "boundary-only" character. In this study, the newly developed dual reciprocity BEM (DRBEM) [25,26] which can avoid the above restrictions was applied to develop a new algorithm to evaluate thermal states of the biological bodies based on the information recorded at the skin surface, i.e. heat flux or temperature. The blood perfusion and the interior temperature distribution were reconstructed without involving any invasive measurement. The extension of the algorithm for the non-linear bioheat model and boundary conditions is also discussed. Various cases were studied to illustrate its applications. This algorithm can be used as an effective tool for thermal diagnostics in medical practices.

2. Numerical method and algorithms

The well-known Pennes equation [27] was used to model heat transfer in the skin tissue:

$$\rho c_p \frac{\partial T}{\partial t} = \nabla \cdot k\nabla T + \omega_b \rho_b c_b (T_a - T) + Q_m + Q_r \tag{1}$$

where, ρ, c_p, and k denote density, specific heat, and thermal conductivity of tissue; ρ_b, c_b are density and specific heat of blood; ω_b (ml/s/ml) blood perfusion rate; Q_m metabolic heat generation; T_a is the supplying arterial blood temperature and T the tissue temperature; Q_r imposed spatial heating.

Without losing generality, constant properties were used except for blood perfusion. Temperature transients due to the imposed heating can be obtained from Eq. (1) as

$$\frac{1}{\alpha}\frac{\partial \theta}{\partial t} = \nabla^2 \theta - \frac{\omega_b \rho_b c_b}{k}\theta + \frac{Q_r}{k} \tag{2}$$

where $\theta(x, y; t) = T(x, y; t) - T(x, y; 0)$ is the temperature elevated above the steady state in a two-dimensional tissue. Shown in Fig. 1, x denotes the tissue depth from the skin surface while y is along the surface. α is the thermal diffusivity of tissue.

DRBEM is a transformation originated from but superior to the traditional BEM. The basic idea is to employ a fundamental solution corresponding to a simpler equation, and to treat the remaining terms as well as other non-homogeneous terms in the original equation, through a procedure which involves a series expansion using global approximation functions and the application of reciprocity principles [25]. Eq. (2) can be re-arranged in the following form,

$$\nabla^2 \theta = b\frac{\partial \theta}{\partial t} + c\theta + d = h(x, y; t) \tag{3}$$

where, $b = 1/\alpha$, $c = \omega_b \rho_b c_b / k$, $d = -Q_r/k$. The solution of Eq. (3) can be composed of

$$\theta = \tilde{\theta} + \hat{\theta} \tag{4}$$

where $\tilde{\theta}$ is the solution of the homogeneous Laplace equation and $\hat{\theta}$ is a particular solution of the Poisson equation, as

$$\nabla^2 \tilde{\theta} = 0 \tag{5}$$

$$\nabla^2 \hat{\theta} = h \tag{6}$$

It is generally difficult to find a solution $\hat{\theta}$ that satisfies Eq. (6) which is a time-dependent second order differential equation. The DRBEM uses a series of particular solution $\hat{\theta}_j$ instead of a single function $\hat{\theta}$ as,

$$\hat{\theta}(r, t) = \sum_{j=1}^{N+L} \gamma_j(t)\hat{\theta}_j(r) \tag{7}$$

where the γ_j are time-dependent coefficients to be determined; r is the distance from the point j to any other point under consideration. N represents the number of boundary nodes and L the number of internal nodes. The number of $\hat{\theta}_j$ used is equal to the total number of nodes in the problem. The following approximation for h is then proposed,

$$h \approx \sum_{j=1}^{N+L} \gamma_j(t) f_j(r) \tag{8}$$

where f_j are approximation functions having polynomial expressions,

$$f = 1 + r + r^2 + \cdots + r^m \tag{9}$$

where $r^2 = r_x^2 + r_y^2$ (r_x, r_y are the components of r in the direction of the x and y axes). Substituting Eqs. (7) and (8) into Eq. (6) gives,

$$\nabla^2 \hat{\theta}_j = f_j \tag{10}$$

Extensive research has shown that use of the first approximation $f = 1 + r$ can produce good results for a wide range of problems [25,26]. In this case, the corresponding $\hat{\theta}$ can be obtained as

$$\hat{\theta}_j(x, y) = \frac{r^2}{4} + \frac{r^3}{9} \tag{11}$$

Substituting Eqs. (8) and (10) into Eq. (3), leads to

$$\nabla^2 \theta = \sum_{j=1}^{N+L} \gamma_j \left(\nabla^2 \hat{\theta}_j\right) \tag{12}$$

Then, the procedure for developing the BEM for the

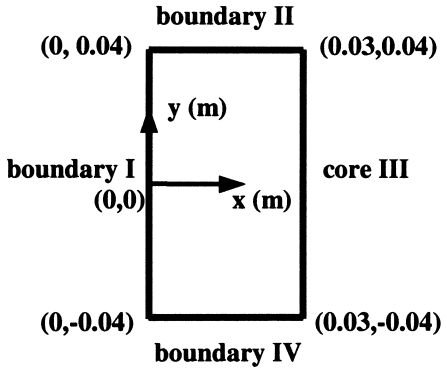

Fig. 1. Boundary definition.

Laplace equation can be applied. Eq. (12) is multiplied by the fundamental solution and integrated over the computation domain, resulting in

$$\int_{\Omega}(\nabla^2\theta)\theta^* \,\mathrm{d}\Omega = \sum_{j=1}^{N+L}\gamma_j\int_{\Omega}\left(\nabla^2\hat{\theta}_j\right)\theta^* \,\mathrm{d}\Omega \tag{13}$$

Integrating by parts the Laplacian terms in Eq. (13) gives the following integral equation for each source node i,

$$C_i\theta_i + \int_{\Gamma} q^*\theta \,\mathrm{d}\Gamma - \int_{\Gamma}\theta^* q \,\mathrm{d}\Gamma = \sum_{j=1}^{N+L}\gamma_j\left(C_i\hat{\theta}_{ij} + \int_{\Gamma} q^*\hat{\theta}_j \,\mathrm{d}\Gamma - \int_{\Gamma}\theta^*\hat{q}_j \,\mathrm{d}\Gamma\right) \tag{14}$$

In two-dimensional cases, the term $\hat{q}_j$ in Eq. (14) is defined as

$$\hat{q}_j = \frac{\partial\hat{\theta}_j}{\partial x}\frac{\partial x}{\partial n} + \frac{\partial\hat{\theta}_j}{\partial y}\frac{\partial y}{\partial n} = \left(r_x\frac{\partial x}{\partial n} + r_y\frac{\partial y}{\partial n}\right)\left(\frac{1}{2} + \frac{r}{3}\right) \tag{15}$$

where n is the unit vector normal to the boundary Γ. It can be seen that Eq. (14) involves no domain integrals. The source term has been substituted by equivalent boundary integrals. Discretizing Eq. (14) and introducing the interpolation functions, it is then integrated over each boundary element and written in terms of nodal values as

$$C_i\theta_i + \sum_{k=1}^{N}H_{ik}\theta_k - \sum_{k=1}^{N}G_{ik}q_k = \sum_{j=1}^{N+L}\gamma_j\left(C_i\hat{\theta}_{ij} + \sum_{k=1}^{N}H_{ik}\hat{\theta}_{kj} - \sum_{k=1}^{N}G_{ik}\hat{q}_{kj}\right) \tag{16}$$

where coefficients $C_i = \beta/2\pi$. β is the internal angle at point i on the radius. The index k is used for the boundary nodes which are the field points. It should be noted that, since $\hat{\theta}$ and $\hat{q}$ are known functions once f is defined, there is no need to approximate their variations within each boundary element. To solve for the coefficient γ, the matrix form of Eq. (8) can be written as:

$$\gamma = F^{-1}h = F^{-1}\left(b\dot{\theta} + c\theta + d\right) \tag{17}$$

where each column of F consists of a vector f_j containing the values of the function f at the $(N+L)$ DRBEM collocation points. Then the matrix form of Eq. (16) becomes

$$H\theta - Gq = \left(H\hat{\Theta} - G\hat{Q}\right)F^{-1}\left(b\dot{\theta} + c\theta + d\right) \tag{18}$$

Letting $S = -(H\hat{\Theta} - G\hat{Q})F^{-1}$ leads to

$$S\left(b\dot{\theta} + c\theta + d\right) + H\theta = Gq \tag{19}$$

The linear approximation will be proposed for the variation of θ, q, and t within each time step, in the form

$$\theta = (1-\theta_u)\theta^m + \theta_u\theta^{m+1} \tag{20a}$$

$$q = \left(1-\theta_q\right)q^m + \theta_q q^{m+1} \tag{20b}$$

$$\dot{\theta} = \frac{1}{\Delta t}\left(\theta^{m+1} - \theta^m\right) \tag{20c}$$

where θ_u and θ_q are parameters which position the values of θ and q, respectively, between time levels m and $m+1$. A series of tests carried out in [25] indicated that, in general, accurate values can be obtained for θ_u and θ_q of 0.5 and 1.0, respectively. Substituting Eqs. (20a)–(20c) into Eq. (19) yields

$$\left(\frac{Sb}{\Delta t} + Sc\theta_u + \theta_u H\right)\theta^{m+1} - \theta_q G q^{m+1} + Sd = \left(\frac{Sb}{\Delta t} - Sc(1-\theta_u) - H(1-\theta_u)\right)\theta^m + \left(1-\theta_q\right)Gq^m \tag{21}$$

Applying the initial condition (IC) and the boundary condition (BC), one can rearrange the left side of Eq. (21) and solve the unknowns θ and q, with respect to time. The algorithm of Eq. (21) can be flexibly used for various applications.

To solve for different bioheat transfer problems involving various boundary conditions and non-linear terms, several issues need to be addressed. For heterogeneously distributed heating $Q_{\mathrm{r}}(x, y)$ and perfusion $\omega_{\mathrm{b}}(x, y)$, calculation can be performed through directly incorporating these terms into the above algorithm without increasing any difficulty. But if these terms are temperature dependent, an iteration is needed. This can be dealt with as illustrated in the following example.

In hyperthermia treatment, blood perfusion increases with tissue temperature approximately following a linear relation as [28]:

$$\omega_{\mathrm{b}} = k_1 + k_2 T \tag{22}$$

where k_1, k_2 are empirical constants. Based on Eq. (1), an algorithm corresponding to Eq. (21) can be obtained as:

$$\left(\frac{Sb}{\Delta t}+Sc'\theta_u+\theta_u H\right)T^{m+1}-\theta_q Gq^{m+1}+Sd'$$
$$=\left(\frac{Sb}{\Delta t}-Sc'(1-\theta_u)-H(1-\theta_u)\right)T^m \quad (23)$$
$$+\left(1-\theta_q\right)Gq^m-Sf'T^2$$

where

$$c'=\frac{k_1\rho_b c_b-k_2\rho_b c_b T_a}{k},\quad d'=-\frac{Q_m+Q_r+k_1\rho_b c_b T_a}{k},$$
$$f'=\frac{k_2\rho_b c_b}{k}.$$

This non-linear transient algorithm due to the occurrence of the $Sf'T^2$ term can be solved through iteration at each time step. Similarly, calculations can be carried out over the entire time period. If blood perfusion appears to be a non-linear function of temperature, i.e. $\omega_b=k_1\exp(k_2T)$ [20], then an algorithm with the non-linear temperature term placed on the right-hand side of Eq. (23) can also be built.

Eq. (21) can be directly used to solve problems under the first (temperature) or second (heat flux) thermal boundary conditions. At the heat convection boundary, it has

$$h_f(\theta-\theta_f)=-k\frac{\partial\theta}{\partial n}=kq \quad (24)$$

where $\theta_f=T_f-T(x,\ y;0),\ (x,y)\in$ the convection boundary.

Eq. (21) becomes,

$$\left(\frac{Sb}{\Delta t}+Sc\theta_u+\theta_u H+\frac{\theta_q h_f}{k}G\right)\theta^{m+1}$$
$$=\frac{\theta_q h_f\theta_f}{k}G-Sd+\left(\frac{Sb}{\Delta t}-Sc(1-\theta_u)\right.$$
$$\left.-H(1-\theta_u)\right)\theta^m+\left(1-\theta_q\right)Gq^m \quad (25)$$

Based on Eqs. (25) and (21), a computer code can be developed to solve for the temperatures at the time step $m+1$.

3. Diagnostics of thermal states of the biological bodies

In non-invasive evaluation of thermal states of the biological bodies, only the dynamic information on the skin surface can be used to extract important physiological parameters, i.e. heterogeneous perfusion field [1]. In our previous study [29], the phase shift of the surface temperature in response to the sinusoidal heating was shown to be related to the local blood perfusion and the heating frequency. But for non-homogeneous blood perfusion frequently encountered in tissues, 1D formulation is not sufficient. In this section, the effect of the spatial variation of blood perfusion on the temporal temperature distribution in a 2D domain given in Fig. 1 will be explored. Additionally, successful detection of the temperature distribution can be used to extract the perfusion condition and thus the physiological state. The DRBEM program developed in this study was first validated by comparing the calculated 1D temperature field with the theoretical solution given in [29].

3.1. Validation of the algorithm

Referring to Fig. 1, a constant core temperature is assumed at boundary III while there is an intentionally exerted sinusoidal heating at I. Boundaries II and IV are treated as adiabatic by assuming that tissue far from the area of interest is not affected by the imposed thermal disturbance.

$$q''(x,y;t)=0,\quad x,y\in II,IV$$

$$q''(x,y;t)=\bar{q}''_w\cos(\omega t),\quad x,y\in I$$

$$\theta(x,y;t)=0,\quad x,y\in III \quad (26)$$

where $\bar{q}''_w$ and ω are amplitude and frequency of the imposed sinusoidal heating at the skin surface, respectively. Typical tissue properties are applied as given in [30]: $\rho=\rho_b=1000$ kg/m^3, $c_p=c_b=4000$ J/kg °C, $k=0.5$ W/m °C.

Fig. 2 shows the transient temperatures at $(x=0,\ y=0)$ under the sinusoidal surface heating of $\bar{q}''_w=250$ W/m^2, $\omega=0.01$. The uniform blood perfusion is $\omega_b=0.0005$ ml/s/ml. It depicts that the numerical

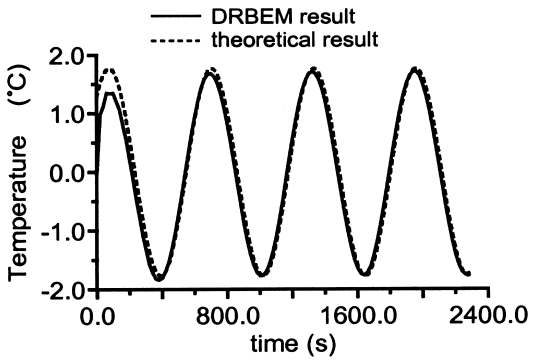

Fig. 2. Validation of the DRBEM code with the theoretical prediction in the 1D case ($\bar{q}''_w=250$ W/m^2, $\omega=0.01$, $\omega_b=0.0005$ ml/s/ml.

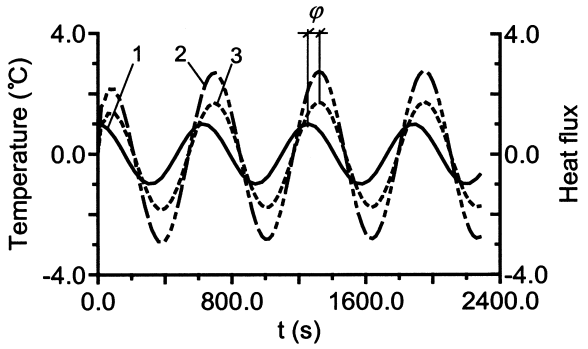

Fig. 3. Transient temperature and heat flux at the skin surface point (0, 0) ($\omega_b = 0.0005$ ml/s/ml, $\omega = 0.01$).

results by DRBEM agree very well with the theoretical calculation except for a small discrepancy (15%) at the early stage of calculation.

Further, temperature responses at the surface ($x = 0, y = 0$) to the respective heating of $\bar{q}''_w = 400$ W/m^2, $\omega = 0.01$ and $\bar{q}''_w = 250$ W/m^2, $\omega = 0.01$ are shown in Fig. 3. The phase shift φ between the heat flux and the temperature profile is clearly illustrated. This shift can be recorded and applied to estimate the local perfusion. The correlation between perfusion and the phase shift has been analytically obtained in [29] as:

$$\omega_b = -\frac{\rho c_p \omega}{\mathrm{tg}(2\varphi)\cdot \rho_b c_b} \tag{27}$$

Here φ is independent of the heating magnitude $\bar{q}''_w$ and its value is read as $\varphi \approx -76 \times \omega = -0.76$. Substituting this value together with $\omega = 0.01$ in Eq. (27), the blood perfusion rate is calculated as $\omega_b = 0.000508$ ml/s/ml. It is very close to the above prescribed value $\omega_b = 0.0005$ ml/s/ml for computation in the whole 2D domain. Under uniform surface heating, heat transfer can be closely approximated as 1D when blood perfusion is homogeneous which is clearly illustrated by the temperature distribution given in Fig. 4. However, if one wishes to estimate the transient heterogeneous blood perfusion, the present approach based on the DRBEM algorithm is necessary. Theoretically, this approach accounts for the dynamic change of the local perfusion concomitant with the external heating or the hypothermic condition. For noninvasive purpose, it is intended to detect the temperature and heat flux information only at the skin surface. Practically, the surface heat flux q^m ($m = 1, 2, \ldots$) is easy to apply. The induced surface temperature responses θ^m ($m = 1, 2, \ldots$) can then be recorded. Thus both the transient heat flux and temperature are known at the skin surface, allowing us to estimate the unknown field $c(x, y; t)$ proportional to blood perfusion based on the above mentioned algorithm. Due to the surface heating, $d = 0$ in Eq. (3). Then, by introducing the initial condition θ^1, q^1 and the following θ^m, q^m, the non-homogeneous $c(x, y; t)$ can be reconstructed through rearranging Eq. (21) as,

$$\begin{aligned} &S\left[\theta_u\theta^{m+1} + (1-\theta_u)\theta^m\right]c \\ &\quad = -\left(\frac{Sb}{\Delta t} + \theta_u H\right)\theta^{m+1} + \theta_q G q^{m+1} \\ &\quad + \left(\frac{Sb}{\Delta t} - H(1-\theta_u)\right)\theta^m + (1-\theta_q)Gq^m \end{aligned} \tag{28}$$

Eq. (28) can be written in a matrix form:

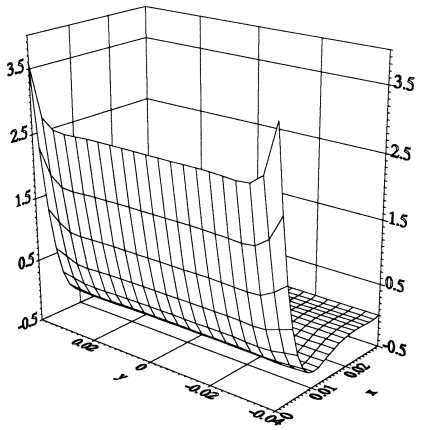

Fig. 4. Temperature distribution in the 2D domain at time $t = 900$ s ($\bar{q}''_w = 400$ W/m^2, $\omega_b = 0.0005$ ml/s/ml, $\omega = 0.01$).

$$AX = F \tag{29}$$

where A is the coefficient matrix, X is the vector to be solved, and F is the constant vector. The blood perfusion field is obtained as $\omega_b(x, y; t) = c(x, y; t)k/\rho_b c_b$. Meanwhile, the interior temperature field can also be reconstructed using Eq. (16).

3.2. Steady state diagnostics of the tumor site

It is known that the abnormal distribution of blood perfusion or metabolic heat generation often lead to different thermal state expressions at the skin surface. This difference is beneficial for noninvasive diagnostics of the physiological state of the biological body. For illustration purpose, the following BCs are applied to the domain shown in Fig. 1,

$$q''(x, y; 0) = 0, \quad x, y \in I, II, IV$$

$$T(x, y; 0) = 37^\circ\text{C}, \quad x, y \in III \tag{30}$$

To avoid the influence from the surrounding environment, the skin boundary is covered with an insulating material long enough to allow the temperature inside the body to reach the steady state. The core temperature is still regarded as constant as well as arterial blood temperature ($T_b = 37^\circ$C). It has long been revealed that existence of a malignant tumor often leads to very different blood perfusion rates in the tumor and the surrounding tissues [31–35]. The metabolic rate in the tumor site often appears abnormally high. Due to a shortage of experimental measurements of these parameters, the following assumptions are made for a highly vascularized tumor situated underneath the skin:

for healthy tissue,

$$\omega_b = 0.0005\ \text{ml/s/ml}, x, y \in \Omega,$$
$$Q_m = 420\ \text{J/m}^3\ \text{s}, x, y \in \Omega \tag{31a}$$

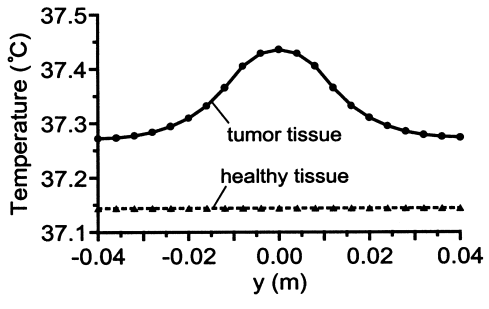

Fig. 5. Comparison of the skin ($x, y \in I$) temperature of two kinds of tissues

for tissue with a tumor,

$$\omega_b = \begin{cases} 0.0005\ \text{ml/s/ml}, & x, y \notin L \\ 0.002\ \text{ml/s/ml}, & x, y \in L \end{cases},$$
$$q_m = \begin{cases} 420\ \text{J/m}^3\ \text{s} & x, y \notin L \\ 4200\ \text{J/m}^3\ \text{s}, & x, y \in L \end{cases} \tag{31b}$$

where $L \subseteq [|y| \le 0.01\ \text{m}, \ 0.005 \le x \le 0.015\ \text{m}]$ is prescribed as tumor domain, Ω is the entire domain given in Fig. 1.

Using the DRBEM algorithm, the steady state surface temperature distributions were reconstructed for both tumor and healthy tissues. Fig. 5 clearly shows the distinct difference between skin temperature distribution due to different blood perfusion and metabolic heat generation. The corresponding spatial temperature profiles are depicted in Fig. 6. The irregularity of temperature distribution is quite visible in Fig. 6(a). The non-homogeneity of the skin surface temperature caused by the abnormal blood perfusion in the subcutaneous tissue may serve as an index for tumor detection in clinics. Given the small magnitude of the temperature difference, high resolution thermal sensors are required for this application.

The most recently developed high resolution thermography can serve as an effective tool for temperature sensing [1–6]. In this case, boundary I (Fig. 1) is exposed to convection and radiation. Radiation at the skin surface can be simplified as a convection-like term when temperature variations are small. Therefore the boundary at I can be expressed as:

$$-K\left.\frac{\partial T}{\partial n}\right|_{\text{skin}} = h_r(T_s - T_{\text{env}}) + h_f(T_s - T_f) \tag{32}$$

where h_r is the apparent radiation heat transfer coefficient, and T_{env} is the environmental background temperature while T_f is the ambient temperature and T_s the skin temperature.

When the environmental temperature varies in a small range, the value of h_r can be estimated as $h_r = \varepsilon\sigma(T^2 + T_{\text{env}}^2)(T + T_{\text{env}})$ (where ε is the skin emissivity, σ is the Stefan–Boltzmann constant) [4]. Under normal conditions, h_r is approximately 6.19 W/m^2 °C. The heat transfer coefficient h_f usually falls between 5 and 25 W/m^2 °C for natural convection. Thus for a preliminary analysis. $h_{\text{eff}} = h_r + h_f = 10$ W/m^2 °C and $T_{\text{env}} = T_f = 25^\circ$C are applied. The convection algorithm Eq. (25) and Eq. (21) are used to solve the thermal fields at the skin surface and inside the body.

Fig. 7 depicts calculations of the temperature and heat flux at the skin surface while it is subject to the convection boundary condition. Fig. 8 shows the temperature distribution within the tissue. Clearly, temperature distributions are different enough to be detectable through infrared thermome-

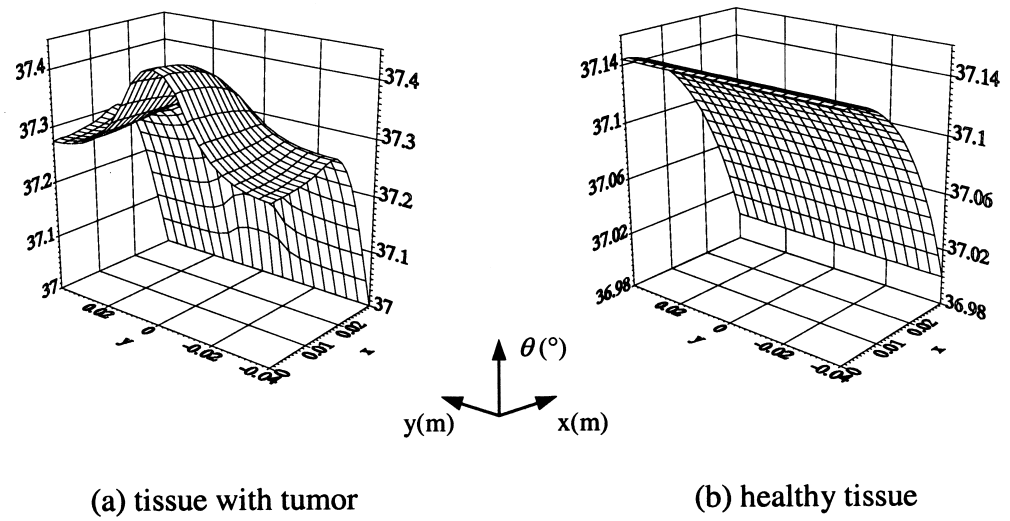

Fig. 6. Steady state temperature distributions.

try. The very different heat flux distribution (Fig. 7b) at this boundary also provides additional information for the diagnosis. Besides, as there is no need for the tissue to reach a new steady state as required in the method mentioned above, this is more practical. For diagnostic clinics, a database of the surface temperature and heat flux corresponding to different thermal states of tissue can be established.

To improve sensitivity, forced convection can be applied to the skin surface. Fig. 9 shows the results calculated under two effective heat transfer coefficient $h_{\text{eff}} = h_{\text{r}} + h_{\text{f}} = 10,\ 30\ \text{W/m}^2\ ^\circ\text{C}$ and $T_{\text{env}} = T_{\text{f}} = 25^\circ\text{C}$. The difference between the highest and lowest temperature can be enlarged by increasing h_{eff}.

One concern is which kind of tumors can be detected through only the surface temperature or heat flux acquisition, and the depth and site of a tumor can be detected. This is in fact restricted by the sensitivity of the surface thermometry and the algorithms applied, and more importantly, understanding of the tumor physiology. Calculations show, as expected, that the closer the tumor is to the surface, the larger is the irregularity in surface temperature or heat flux distribution. Detailed studies need to be performed to correlate the diseased state to the thermal state of tissue in clinics.

3.3. Dynamic burn evaluation

Accurate early assessment of skin damage in a burn injury can greatly improve post care [21,36–43]. It has

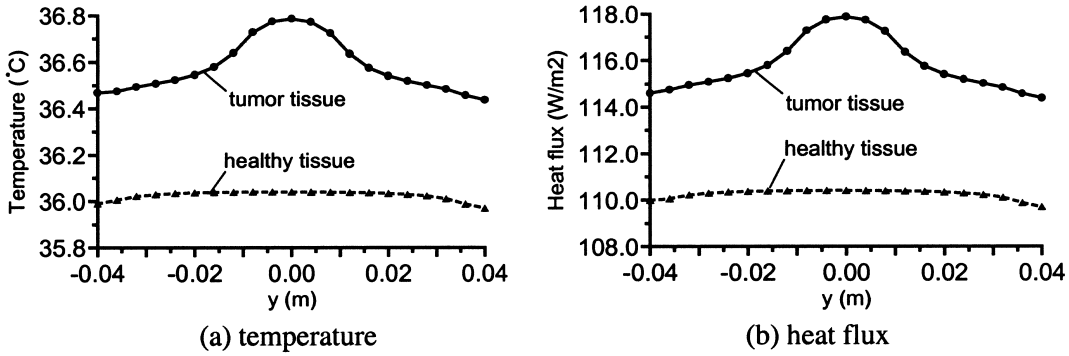

Fig. 7. Comparison of the skin ($x, y \in I$) temperature and heat flux profiles ($h_{\text{eff}} = 10\ \text{W/m}^{2\circ}\text{C}$, and $T_{\text{f}} = T_{\text{env}} = 25^\circ\text{C}$).

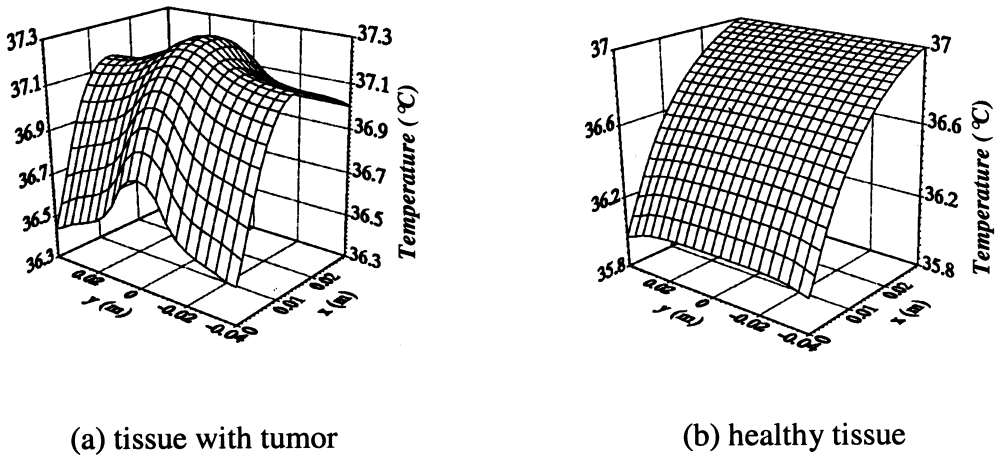

(a) tissue with tumor (b) healthy tissue

Fig. 8. Steady state temperature distributions.

been found that burns cause changes in blood flow and heat conduction of skin depending on the degree of burn. Successful detection of changes in the thermal properties of skin can be used for burn evaluation. Applying a pulse heating to the skin surface, the temperature response is expected to be different in normal and burned tissues. For preliminary comparison, the normal and burned tissues have been defined with homogeneous heat conductivity and blood perfusion, but of different values (normal tissue: $k = 0.5$ W/m °C, $\omega_b = 0.0005$ ml/s/ml; burned tissue: $k = 0.2$ W/m °C, $\omega_b = 0.0001$ ml/s/ml). Lower values of thermal conductivity and blood perfusion are used for burned tissues considering possible loss of water in the tissue and damage to the vascular bed by burning. Calculations shown in Fig. 10 demonstrate a very different transient temperature profile at the skin surface for the two types of tissue. Compared to the quantitative evaluation through color analysis of the skin surface [40–43], the present approach possesses the advantage of simplicity.

From our previous study [29], the temperature decay of the skin after being heated by a constant surface power is determined by an exponential term $\exp(-\omega_b \rho_b c_b t/\rho c_p)$ in which perfusion plays an important role. This has also been shown by Arkin et al. [44] and Diederich et al. [45] in analyzing pulse heating inside tissues. Thus through exerting a heating pulse on the skin surface and evaluating the time constant (which can be regarded as a diagnostic index) for surface temperature decay, the properties of the skin can be obtained for the evaluation of burn injury. Fig. 11 shows the temperature evolution in burned and healthy

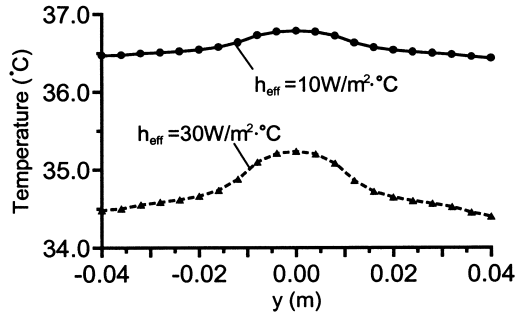

Fig. 9. Comparison of temperatures at the skin surface (tissue with a tumor) under different convection coefficients.

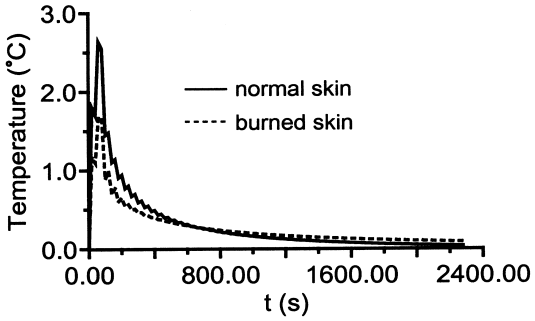

Fig. 10. Temperature response in skin surface point ($x = 0, y = 0$) under; pulse heating $q'' =$

$$\begin{cases} 0 & x = 0,\ |y| > 0.01\,\text{m} \\ 400\,\text{W/m}^2 & x = 0,\ |y| \le 0.01\,\text{m}; \end{cases}$$

normal tissue; $k = 0.5$ W/m °C, $\omega_b = 0.0005$ ml/s/ml; burned tissue: $k = 0.2$ W/m °C, $\omega_b = 0.0001$ ml/s/ml.

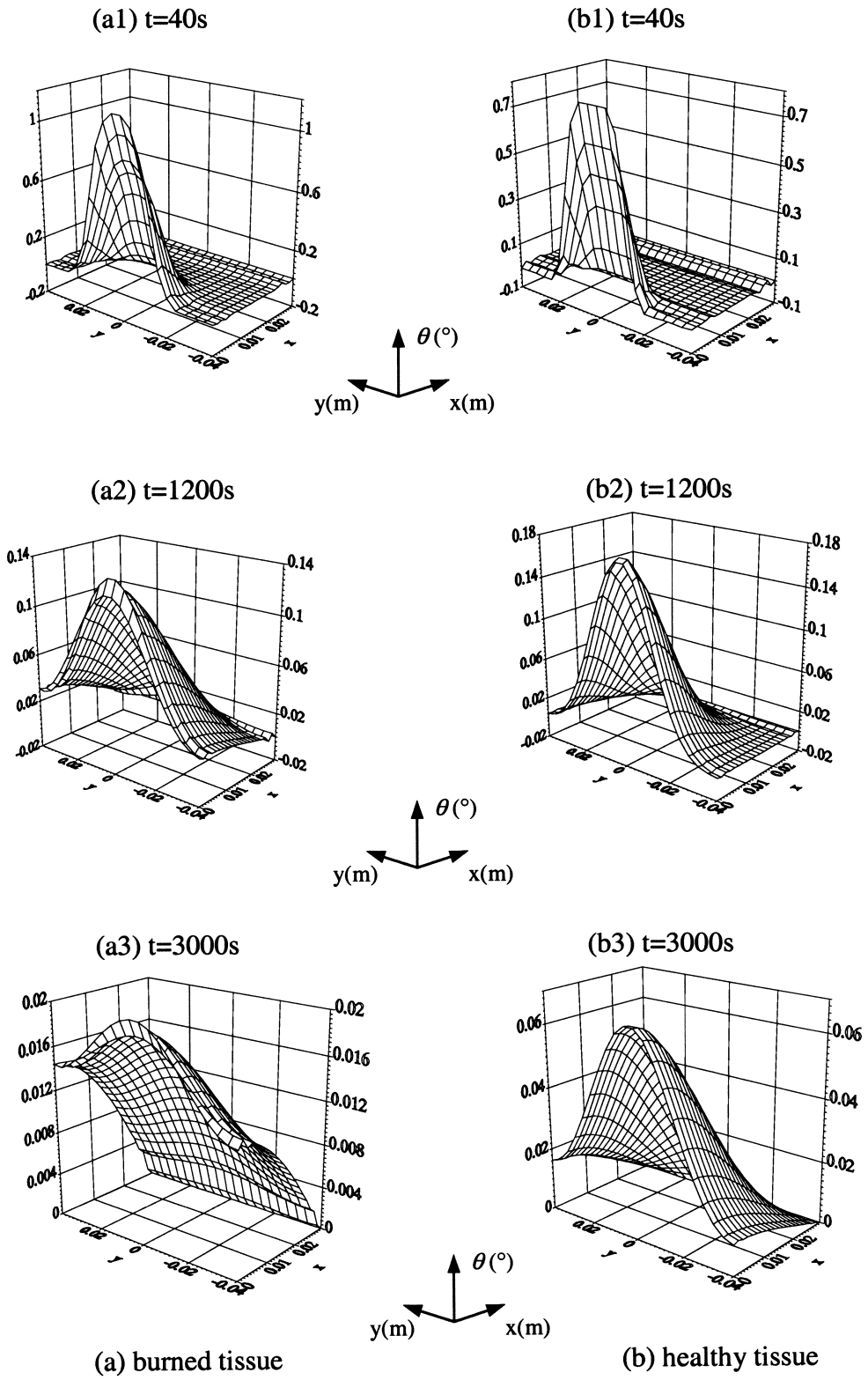

Fig. 11. Temperature evolution in two tissues under pulse surface heating.

tissues under surface pulse heating. The difference in magnitude and profile is distinct.

4. Discussion and conclusion

The geometry and properties of biological bodies vary drastically, which make the analysis of bioheat transfer rather complicated. Studies on thermal states of the biological bodies may be carried out as follows: (1) Determination of system parameters, such as the living tissue thermal conductivity, specific heat, blood perfusion, metabolic rate; (2) Solution to direct problems with known parameters like temperature prediction for heating planing in hyperthermia based on the power input; (3) Solution to inverse problems using measurable variables of the system to infer the unknown system parameters; and (4) Solution to the mixed problem using part of the measured system parameters and the variables to estimate other unknown parameters and variables, such as the simultaneous determination of blood perfusion, spatial heat source, and the temperature field. Obviously, problem (4) appears more complicated, yet is common in reality. As has been shown above, the DRBEM is capable of solving most of the above mentioned problems. It provides a generalized numerical approach for identifying thermal states of the biological bodies for different purposes. More importantly, the method presented in this paper can be used to solve an inverse heat transfer problem without internal grid generation, which is one of its distinctive merits in comparison to most of other numerical methods.

In hyperthermia treatment for tumors, spatial heating exists and determination of the specific absorption rate (SAR) of heat in the tissue is generally very complicated. Methods used to determine the SAR for typical heating, like microwave, radio-frequency etc., are in fact obtained through a curve fit to the measured temperatures [46]. However, as has been pointed out, due to the highly non-homogeneous properties of the biological bodies, the SAR is both location and time dependent. The present algorithm can be used to determine the temporal distribution of SAR during heating. For this application, variables in Eq. (21) are $c(x, y; t)$ and $d(x, y; t)$. If enough boundary heat flux and temperature information is recorded at each time step, then the unknown c and d can be solved. But it should be noted that the inverse problem involving solution of Eq. (29) generally appears ill-posed [24]. Thus only by incorporating some techniques like Tikhonov's regularization method [47] can the equation be appropriately solved. The number of values to be determined depends on the number of knowns at the skin surface. The simulations performed herein are based on very idealistic boundary conditions. Three-dimensional modeling is required to reveal temperature behaviors over the skin surface when more complex BCs are encountered in actual circumstances.

Comprehensive analysis of the irregular thermal state at the skin surface and its correlation to the abnormal circulation or metabolic rate in tissue underneath is rather complex. As discussed in [1], although a unique three-dimensional perfusion field can be reconstructed through a series of two-dimensional imaging at the skin surface when subjected to dynamic changes in the thermal state, the depth of the detectable field is dependent on the sensitivity and speed of the IR imaging system. Above all, correlations of the thermal information at the skin boundary to the abnormal physiological parameters, i.e. circulation or metabolic rate in tissues, are imperative for application of the boundary information based diagnostics in clinics.

To date, diagnostics of the material properties based on observation of thermal signals on the surface of an object has been extensively investigated [48–52]. Recently, a series of papers about thermal infrared medicine were published in the journal of IEEE Engineering in Medicine and Biology [July/Aug., 1998]. Enhancement of the difference in surface thermal pictures between diseased and healthy tissues is the key to improving diagnostic accuracy. The DRBEM algorithm developed in this research can be viewed as one of the promising approaches. Its potential value depends upon whether the boundary temperature and heat flux can be accurately measured at the same time to non-invasively reconstruct the internal perfusion field that is of great importance in clinical practices. In the case of uniform blood perfusion, other methods can also be used as discussed earlier. However, blood perfusion is expected to be heterogeneous at the scale of small vessels and capillaries. The heterogeneity can not be easily resolved due to the limitation of the current measuring techniques. The present method has potential to provide point by point estimation of perfusion non-invasively.

Acknowledgements

This work was partially supported by the National Institute of Health 7 R29 CA 67970-04.

References

[1] M.M. Chen, C.O. Pedersen, J.C. Chato, On the feasibility of obtaining three-dimensional information from thermographic measurements, ASME Journal of Biomechanical Engineering 99 (1977) 58–64.

[2] J.C. Chato, Measurement of thermal properties of biological materials, in: A. Shitzer, R.C. Eberhart (Eds.), Heat Transfer in Medicine and Biology, vol. I, Plenum Press, New York, 1985, pp. 167–173 (Chapter 8).
[3] H.F. Bowman, Estimation of tissue blood flow, in: A. Shitzer, R.C. Eberhart (Eds.), Heat Transfer in Medicine and Biology, vol. I, Plenum Press, New York, 1985, pp. 193–230 (Chapter 9).
[4] J.C. Chato, Fundamentals of Bioheat Transfer, Springer-Verlag, Berlin, 1989.
[5] M. Gautherie, Clinical Thermology, Subseries Thermotherapy, vol. 1-4, Springer-Verlag, Heidelberg, 1990.
[6] M. Miyakawa, J.C. Bolomey (Eds.), Non-Invasive Thermometry of the Human Body, CRC Press, Boca Raton, 1996.
[7] S.T. Clegg, T.V. Samulski, K.A. Murphy, G.L. Rosner, M.W. Dewhirst, Inverse techniques in hyperthermia: a sensitivity study, IEEE Transactions on Biomedical Engineering 41 (1994) 373–382.
[8] N. Tsuda, K. Kuroda, Y. Suzuki, An inverse method to optimize heating conditions in RF-capacitive hyperthermia, IEEE Transations on Biomedical Engineering 43 (1996) 1029–1037.
[9] Y. Rabin, A. Shitzer, Combined solution of the inverse Stefan problem for successive freezing/thawing in non-ideal biological tissues, ASME Journal of Biomechanical Engineering 119 (1997) 146–152.
[10] C.T. Liauh, S.T. Clegg, R.B. Romer, Estimating three-dimensional temperature fields during hyperthermia: studies of the optimal regularization parameter and time sampling period, ASME Journal of Biomechanical Engineering 113 (1991) 230–238.
[11] C.T. Liauh, R.B. Romer, Multiple minima in inverse hyperthermia temperature estimation problems, ASME Journal of Biomechanical Engineering 115 (1993) 239–246.
[12] M.M. Osman, E.M. Afify, Thermal modeling of the normal woman's breast, ASME Joural of Biomechanical Engineering 106 (1984) 123–130.
[13] M.M. Osman, E.M. Afify, Thermal modeling of the malignant woman's breast, ASME Journal of Biomechanical Engineering 110 (1986) 269–276.
[14] Y. Rabin, A. Shitzer, Numerical solution of the multidimensional freezing problem during cryosurgery, ASME Journal of Biomechanical Engineering 120 (1998) 32–37.
[15] G.T. Martin, M.G. Haddad, E.G. Cravalho, H.F. Bowman, Thermal model for the local microwave hyperthermia treatment of benign prostatic hyperplasia, IEEE Transactions on Biomedical Engineering 39 (1992) 836–844.
[16] C.F. Babbs, N.E. Fearnot, J.A. Marchosky, C.J. Moran, J.T. Jones, T.D. Plantenga, Theoretical basis for controlling minimal tumor temperature during interstitial conductive heat therapy, IEEE Transactions on Biomedical Engineering 37 (1990) 662–672.
[17] D.Y. Yuan, J.W. Valvano, E.N. Rudie, L.X. Xu, 2-D finite difference modeling of microwave heating in the prostate, Advances in Heat and Mass Transfer in Biotechnology, ASME HTD-vol. 322/BED-vol. 32, 1995, pp. 107–113.
[18] W.H. Newman, G.T. Martin, D.A. Sidney, Evaluation and application of the basis element method: a rapid, 3-D algorithm for bioheat transfer calculations, Advances in Heat and Mass Transfer in Biotechnology, ASME HTD-vol. 322/BED-vol. 32, 1995, pp. 49–54.
[19] C.K. Charny, R.L. Levin, A three-dimensional thermal and electromagnetic model of whole limb heating with a MAPA, IEEE Transactions on Biomedical Engineering 38 (1991) 1030–1039.
[20] B.M. Kim, S.L. Jacques, S. Rastegar, S. Thomsen, M. Motamedi, Nonlinear finite-element analysis of the role of dynamic changes in blood perfusion and optical properties in laser coagulation of tissue, IEEE Journal of Selected Topics in Quantum Electronics 2 (1996) 922–932.
[21] K.R. Diller, L.J. Hayes, Analysis of tissue injury by burning: comparison of in situ and skin flap models, Int. J. Heat Mass Transfer 34 (1991) 1393–1406.
[22] A.M. Kleinman, R.B. Roemer, A direct substitution, equation error technique for solving the thermographic tomography problem, ASME Journal of Biomechanical Engineering 105 (1983) 237–243.
[23] C.L. Chan, Boundary element method analysis for the bioheat transfer equation, ASME Journal of Biomechanical Engineering 114 (1992) 358–365.
[24] Z.P. Ren, J. Liu, C.C. Wang, Boundary element method (BEM) for solving normal or inverse bio-heat transfer problem of biological bodies with complex shape, Journal of Thermal Science 4 (1995) 117–124.
[25] P.W. Partridge, C.A. Brebbia, L.C. Wrobel. The Dual Reciprocity Boundary Element Method, Elsevier Applied Science, London, 1992, pp. 69–81, 175–187.
[26] D. Frayce, R.E. Khayat, A. Derdouri, A dual reciprocity boundary element approach to three-dimensional transient heat conduction as applied to materials processing, Numerical Heat Transfer, Part A 29 (1996) 243–264.
[27] H.H. Pennes, Analysis of tissue and arterial temperatures in the resting human forearm, Journal of Applied Physiology 1 (1948) 93–122.
[28] L.X. Xu, L. Zhu, K.R. Holmes, Thermoregulation in the canine prostate during transurethral microwave hyperthermia, part II: blood flow response, Int. J. Hyperthermia 14 (1998) 65–73.
[29] J. Liu, L.X. Xu, Estimation of blood perfusion using phase shift in temperature response to sinusoidal heating at the skin surface, IEEE Transactions on Biomedical Engineering 46 (1999) 1037–1043.
[30] K.R. Holmes, Biological structures and heat transfer, report from the Allerton Workshop on the Future of Biothermal Engineering, 1997.
[31] C.W. Song, Physiological factors in hyperthermia, National Cancer Institute Monograph 61 (1980) 169–176.
[32] C.W. Song, J.G. Rhee, S.H. Levitt, Blood flow in normal tissues and tumors during hyperthermia, JNCL 64 (1980) 119–124.
[33] C.W. Song, A. Lokshina, J.G. Rhee, M. Patten, S.H. Levitt, Implication of blood flow in hyperthermic treatment of tumors, IEEE Transactions on Biomedical Engineering 31 (1984) 9–16.

[34] C.W. Song, M.S. Kang, J.G. Rhee, M. Patten, S.H. Levitt, The effect of hyperthermia on vascular function, pH, and cell survival, Radiation Biology 137 (1980) 795–803.
[35] T.E. Dudar, R.K. Jain, Differential response of normal and tumor microcirculation to hyperthermia, Cancer Research 44 (1984) 605–612.
[36] D.A. Torvi, J.D. Dale, A finite element model of skin subjected to a flash fire, ASME J. of Biomechanical Engineering 116 (1994) 250–255.
[37] F.S. Knox III, T.L. Wachtel, G.R. McCahan, S.C. Knapp, Thermal properties calculated from measured water content as a function of depth in porcine skin, Burns 12 (1986) 556–562.
[38] T.A. Brans, R.P. Dutrieux, M.J. Hoekstra, R.W. Kreis, J.S. du pont, Histopathological evaluation of scalds and contact burns in the pig model, Burns 20 (1994) S48–51.
[39] M.C. Schellpfeffer, M. Toner, R.C. Lee, R.D. Astumian, Advances in the evaluation and treatment of electrical and thermal injury emergencies, IEEE Transactions on Industry Applications 31 (1995) 1147–1152.
[40] H.A. Green, D. Bua, R.R. Anderson, N.S. Nishioka, Burn depth estimation using indocyanine green fluorescence, Arch Dermatol 128 (1992) 43–49.
[41] M.A. Afromowitz, J.B. Callis, D.M. Heimbach, L.A. Desoto, M.K. Norton, Multispectral imaging of burn wounds: a new clinical instrument for evaluating burn depth, IEEE Transactions on Biomedical Engineering 35 (1988) 842–849.
[42] M.A. Afromowitz, G.S. van Liew, D.M. Heimbach, Clinical evaluation of burn injuries using an optical reflectance technique, IEEE Transactions on Biomedical Engineering 34 (1987) 114–123.
[43] G.L. Hansen, E.M. Sparrow, J.Y. Kokate, K.J. Leland, P.A. Iaizzo, Wound status evaluation using color image processing, IEEE Transactions on Medical Imaging 16 (1997) 78–86.
[44] H. Arkin, K.R. Holmes, M.M. Chen, W.G. Bottje, Thermal pulse decay method for simultaneous measurement of local thermal conductivity and blood perfusion: a theoretical analysis, ASME Journal of Biomechanical Engineering 108 (1986) 208–214.
[45] C.J. Diederich, S. Clegg, R.B. Roemer, A spherical source model for thermal pulse decay method of measuring blood perfusion: a sensitivity analysis, ASME Journal of Biomechanical Engineering 111 (1989) 55–61.
[46] L. Zhu, L.X. Xu, N. Chencinski, Quantification of the 3-D electromagnetic power absorption rate in tissue during transurethral prostatic microwave thermotherapy using heat transfer model, IEEE Transactions on Biomedical Engineering 45 (1998) 1163–1172.
[47] A.H. Tikhonov, in: Solution of Ill-Posed Problems, Geography Press, Beijing, 1979 (in Chinese, translated from Russian).
[48] D. Wei, G.M. Saidel, S.C. Jones, Optimal design of thermistor probe for surface measurement of cerebral blood flow, IEEE Transations on Biomedical Engineering 37 (1990) 1159–1172.
[49] D. Wei, G.M. Saidel, S.C. Jones, Estimation of cerebral blood flow from thermal measurement, ASME Journal of Biomechanical Engineering 117 (1995) 74–85.
[50] M.B. Suddendorf, M.G. Somekh, M. Liu, Thermal wave probe microscopy for materials characterization, Int. J. Electronics 77 (1994) 71–76.
[51] L. Pottier, Micrometer scale visualization of thermal waves by photoreflectance microscopy, Appl. Phys. Lett 64 (1994) 1618–1619.
[52] R.E. Imhot, D.J.S. Birch, M.M. Moksin, J.F. Webb, P.H. Willson, T.A. Strivens, Thermal wave NDE, British Journal of NDT 33 (1991) 172–176.